AI-Supported Prediction of Femtosecond Laser Micromachining Parameters

Céline Petit [*1], Nathanaël Mariaule[2], Sven Wauters[2], Arnaud de Decker[2], and David Bruneel[1]

[1]*Lasea, rue Louis Plescia 31, 4102 Seraing, Belgium*
[2]*SAGACIFY, Avenue de Broqueville 12, 1150 Woluwe-Saint-Pierre, Belgium*
[*]*Corresponding author's e-mail: cpetit@lasea.com*

In laser micromachining, the complexity and non-linearity of laser-matter interactions prevent theoretical models from fully predicting experimental results. Consequently, optimizing processes traditionally requires extensive empirical testing, consuming time and resources. We propose an artificial intelligence (AI) based method to determine optimal femtosecond laser micromachining parameters, where a wide range of engraving parameters are used as inputs and quality and dimensional criteria of a machining profile (depth, width, burrs, angles, and surface roughness) are predicted as outputs. Our approach combines an experimental database generated through automated data collection with an AI approximation model and a genetic algorithm. Tested on 316L stainless steel, we evaluate two AI models: XGboost and neural network. The XGboost model outperforms the neural network, achieving lower mean absolute errors (e.g., 1.6 µm vs 3.2 µm for depth, 52 µm vs. 362 µm for width, and 4.9° vs. 22.1° for angle). Compared to LS-Plume®, a physics-based laser machining simulator, our AI system improves depth and angles predictions by 24% and 3%, respectively. It also predicts surface roughness and burr formation. By reducing the need for empirical testing for each new process, our approach enhances precision, efficiency, and adaptability in laser micromachining, offering reliable alternative to trial-and-error methods.
DOI: 10.2961/ilmn.2025.02.2003
Keywords: laser micromachining, optimal parameters prediction, artificial intelligence, femtosecond laser, machine learning model

1. Introduction

In the late 20th century, the commercialization of femtosecond lasers gave rise to an explosion in their use in many industrial fields. The advantage of this new technology is the quasi-non-thermal laser-matter interaction for optimized laser parameters [1]. This characteristic comes from the ultrashort pulses delivered by femtosecond lasers and leads to machining with high quality and excellent repeatability. These high performances can be found for numerous types of materials: metals, ceramics, polymers, and semi-conductors [2-6]. The wide range of materials that can be processed by laser allows to touch on many areas such as biomedical, watch industry, and electronics industry. Each field requires a specific process, mainly surface texturing [7], laser cutting [8], and laser drilling [9], whose quality and performance have been improved with the arrival of ultrafast lasers [10]. However, for each new developed process in a particular field of application, a search of laser parameters must be carried out to achieve an optimum in terms of quality and cycle time. The number of machining parameters that can be adjusted can quickly become large. Indeed, in general, around eight parameters, such as energy per pulse, frequency, and engraving speed, can be modified. Each of these parameters have several accessible values. Consequently, the search of optimal parameters to achieve a machining profile with desired properties, for example depth and surface roughness, requires numerous tests often in the form of squares grouped into matrices for which a different laser parameter is varied in both directions. This step is demanding in terms of operator time and samples and must be repeated for each new process to be achieved. Some tools for simulating machining profiles based on laser parameters already exist [11,12]**.** However, the validity of the results is limited since some effects, such as thermal effects, are not considered or simulators do not apply to all laser processes. Furthermore, this approach remains iterative in the sense that it is necessary to encode a set of laser parameters to obtain the machining profile. In this context, recent advances in artificial intelligence (AI) in many fields increasingly involve the use of this new tool in the world of laser micromachining. In general, machine learning models, among the most popular, the XGboost [13] and the neural network [14], are trained with real data to find a function that describes the studied physical system. This function can then be used to predict the geometry and the quality of the laser engraving from the machining parameters and obtain optimal laser parameters for different materials and various laser processes [15-17].

The goal of the presented work is to obtain an AI model to predict a small number of optimal laser parameters based on dimensions and quality criteria without having to carry out numerous empirical tests for each new process to develop. Some sets of predicted parameters will be directly rule out by an experienced user and the other part will be a starting point to obtain an optimized process. This method will significantly reduce the time required to obtain optimal

machining parameters and will improve the quality of the engravings. The method is based on the combination of an experimental results database and an automated learning step using an AI approximation model and a genetic algorithm to obtain a comprehensive database. Our experimental database considers many input parameters, including the laser parameters, the machining properties, but also the properties of the material to be machined, as well as parameters specific to the laser-matter interaction such as threshold fluence, incubation coefficient, penetration depth, and complex refractive index of the material. Incorporating these variables enables comprehensive AI learning and the prediction of optimal laser machining parameters, for example energy per pulse, scanning speed, number of passes, and pitch to achieve targeted machining meeting dimensional but also quality criteria. These output parameters are the profile depth, width, and angles as well as the surface roughness S_a. We present a case of study demonstrating the prediction of machining properties for 316L stainless steel. A discussion of the performance obtained with both algorithms (XGboost and Neural network) is presented. We also made a comparison between the predictions of our profile simulator LS-Plume® and the AI model. It allows to evaluate the advantage that artificial intelligence can provide compared to simulators based on physical laws.

2. Methods

The physics describing the laser-matter interaction during a femtosecond laser machining is complex and accompanied by stochastic phenomena. Consequently, the modeling and prediction of optimal laser parameters is not an easy task and the artificial intelligence model training requires a large amount of real data. In addition, the number of data to provide in order to train the model increases exponentially with the number of varied laser parameters. Therefore, to propose a model of artificial intelligence (AI) for the prediction of optimal machining parameters, two strategies were adopted: restricting the field of engraving parameters explored by real data and the development of an automated data generation procedure to guarantee enough data for the machine learning phase within the explored parameters window. The proposed procedure is carried out in three main steps: generation of random laser parameters sets with a python script, engraving of squares grouped in matrix on the sample, and measuring the topology properties of each machined square. These properties are used for the training of the AI model. Fig. 1 depicts the workflow adopted to feed the machine learning system. The result of the model training is the identification of optimal laser parameters to meet dimensional and quality criteria of an optimized process in our case of study: 316L stainless steel.

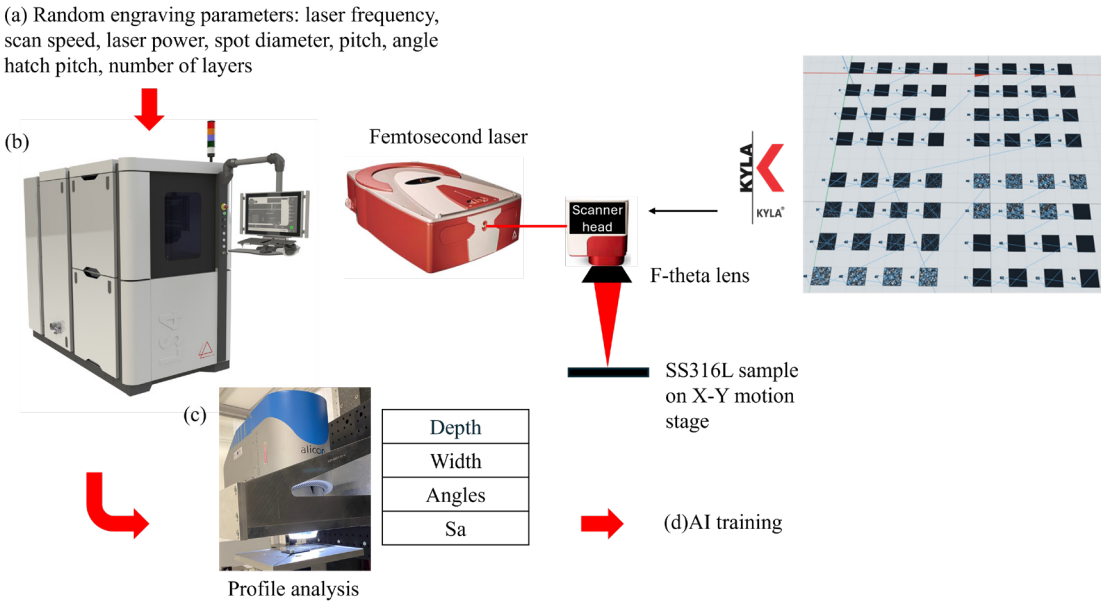

Fig. 1 Illustration of the real data production workflow. (a) A python script generates random engraving parameters sets, (b) each parameter set is loaded in the software Kyla® to engrave squares of 1x1 mm² grouped into matrix, each square is engraved with an unique parameter set, Kyla® controls a Lasea LS4 machine equipped with a Satsuma® laser for the squares machining, (c) each square surface roughness S_a and profile are provided by an Alicona microscope and the profile is analyzed by a python script to obtain profile properties (depth, width, and angles), and (d) these properties are used to train the AI model.

2.1 Real data production

The real data were produced with a Lasea LS4 machine equipped with a satsuma® femtosecond laser from Amplitude systèmes with a radiation wavelength centered at 1030 nm, a power of 20 W at 500 kHz, and a pulse duration of 259 fs. Two spot sizes ω_0 were available thanks to a beam expander and a lens with a focal length of 100 mm. A homemade embedded microscope equipped with an IDS UI-5490SE camera allows an accurate measurement of the two spot diameters at the focal plane: 14 µm and 26 µm at $1/e^2$.

Each data corresponds to a square engraved with a random input parameters combination formed by usual parameters used in the world of micromachining and considers the majority of variables that can be chosen during laser micromachining: laser frequency, laser power, laser spot diameter, spacing of machining lines (pitch), number of machining layers, and angle between each layer (angle hatch pitch). Five laser repetition rates were explored: 100,

125, 166.7, 250, and 500 kHz. The scanning speed was adjusted in the range 50 to 2000 mm/s by step of 50 mm/s. Pitch values were set to one of 5, 7, and 12 µm for the 14 µm spot diameter and to one of 5, 10, 15, and 20 for the 26 µm spot diameter. These values were chosen to test various overlaps. The explored input parameters are summarized in Table 1.

Table 1 Range of parameters for the real data production

Laser parameters	Values
Frequency (kHz)	100, 125, 166.7, 250, 500
Scan speed (mm/s)	50 to 2000, step 50
Power (% of 13.6 W)	30 to 80, step 5
Spot diameter (µm)	14 and 26
Pitch (µm)	5, 7, 12 (for ω_0=14 µm)
	5, 10, 15, 20 (for ω_0=26 µm)
Angle hatch pitch (°)	53, 241
Number of layers	5, 10, 20

A python script has been developed to form random set of input parameters. Each engraving parameters set is loaded into the Lasea machining software Kyla® and will be used to machine a square. These squares are machined by 40x40 matrix on 316L stainless steel sample. The dimensions of each square is fixed to 1x1 mm². The choice of the square dimension is based on a comparison of the machining profiles obtained for square dimensions of 1x1 mm² and 5x5 mm². The experimental study highlighted that the engraving of 1x1 mm² squares does not significantly modify the machining profiles obtained with identical laser parameters. Given the large quantity of data, each square is machined with a unique identification number in order to guarantee traceability of the engraving.

2.2 Real data analysis

The data analysis corresponds to the second step of the automated data generation procedure and allows to obtain output parameters characterizing the machining profiles of each square. Before measurement, each stainless steel sample on which 1600 squares have been engraved is immersed in an ultrasonic bath of distilled water heated to 60 degrees celsius for approximately 8 min. The surface analysis is performed with an Alicona-Infinite Focus SL optical microscope and a x20AX objective with a vertical resolution of 60 nm. A python script was developed to automate the positioning of each square of the 40x40 matrix in the center of the microscope field and to launch an acquisition. To obtain the machining profile, the Alicona carries out two measurements of 1 mm² distributed over each square. At the end of each measurement, a machining profile averaged over a width of 200 µm is obtained as well as the surface roughness measured on a central region of roughly 0.64 mm² in the laser treated squares. Given that the engraving parameters for each square were generated randomly, the settings of the microscope, such as brightness, were chosen to be suitable for the greatest number of cases. This can cause an error in the measurement of extreme cases such as depths greater than 50 µm depending on the surface condition of the engraving background. A Python script performs an analysis to extract a profile and, consequently, the properties of the profile: depth, width, angles, and burrs. The angle 1 and angle 2 correspond to the angle between the vertical and the slope of the machining profile for the left and right side of the profile, respectively. The burr 1 and burr 2 correspond to the burr for the left and right side of the machining profile, respectively. The python script triggers a warning if a problem occurred during the profile determination. This can happen in cases where, for example, the engraving surface roughness is extremely high, making it difficult to evaluate the engraving depth. Fig. 2 shows an example of acquisition results with the Alicona and the simulated profile from the measured profile.

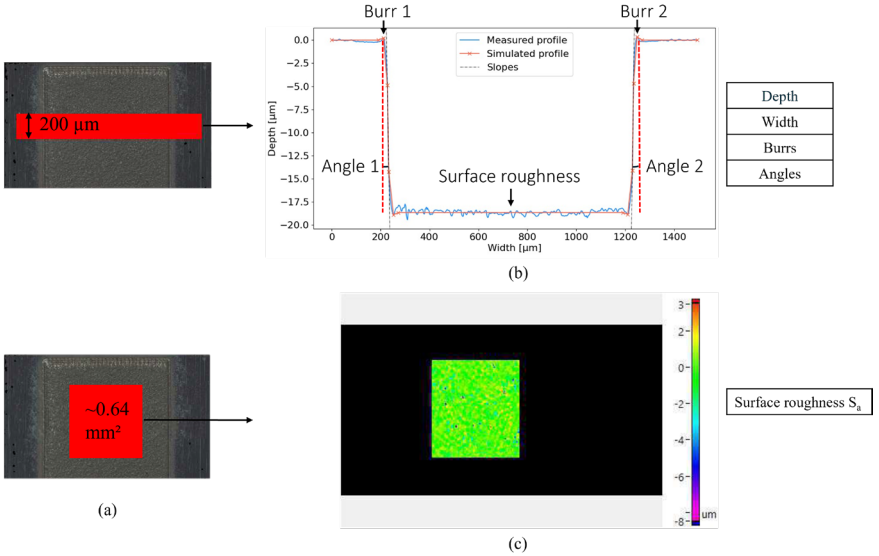

Fig. 2 Example of acquisition result with the Alicona microscope and python script for a machining square with a laser repetition rate of 500 kHz, laser power of 5.8 W, spot diameter of 14 µm, scan speed of 450 mm/s, hatch pitch of 7 µm, angle hatch pitch of 53°, and a number of layers of 10. (a) In red, the region with a width of 200 µm over which the profile is averaged and a region with a size of 0.64 mm² for the surface roughness measurement. (b) Measured profile and simulated profile obtained with a python script to extract the depth, the burrs size, and the angles. (c) Surface roughness measurement S_a.

2.3 AI training

To find the optimal parameters i.e engraving parameters to achieve a machining profile with desired properties, we proceed in two steps. The first phase consists of obtaining an approximation model of the engraving parameters input/output function by using two types of AI algorithms: the XGboost and the neural network. The second phase corresponds to the finding of good candidates of optimal parameters by solving an optimization problem under constraints with a genetic algorithm. It is important to note that due to the heuristic nature of both steps, we are not guaranteed to find the best set of parameters in the space of settings defined by the parameters presented in Table 1. However, this process is sufficient to propose a set of good candidates that can be validated either by humans or through experiments.

In our context, the main principle of machine learning is to find a good approximation function of the studied physical system. Our goal is to determine, within a family of functions, the best approximation of the function that maps our inputs to our outputs. For this purpose, we use statistical algorithms and a dataset of input/output samples from our map. The domain on our function is 10 dimensional and takes for inputs the parameters listed in Table 1, except power (%), together with other physical quantities that can be computed from them or measured: power on the sample (W), the pulse energy (µJ), the peak fluence (J/cm²), the spot diameter (µm), and the physical machining time of a square (s) computed by the number of machined layers divided by the product of the scanning speed and the pitch for a 1x1 mm² square. The image is 7 dimensional with outputs corresponding to the values that we aim to evaluate: depth (µm), width (µm), angles (°), one on each side of the machining profile, the surface roughness (µm) and the burrs (µm), one on each side of the engraving profile. The Fig. 3 and Fig. 4 present histogram plots illustrating the frequency distribution of the input and output parameters of the AI algorithm, respectively.

The most basic version of an AI system is the linear regression, where one finds the affine map that minimizes the mean squared error of a given dataset. We employ richer families of functions: ensemble trees (XGboost) and neural networks. Both of these families are universal approximators, meaning they can approximate any continuous function on a compact set.

The ensemble tree consists of piecewise simple functions (constant or linear). Neural networks are constructed using compositions of linear maps and activation functions such as Rectified Linear Units (ReLU), sigmoid, and hyperbolic tangent.

For the boosting tree, we used the XGboost Python package implementation with 50 estimators, a maximum depth of 5, and default values for the other parameters. These hyperparameter values have been selected using a grid search during the data collection phase of the training set. Tested hyperparameters are: maximum depth in the interval [3,11], minimum sum of instance weight (hessian) needed in a child (min_child_weight) in the interval [1,6], number of trees (n_estimators) in the interval [10, 200], subsample ratio of the training instances in the interval [0.5, 0.7, 1], and learning rate in the interval [0.1, 0.01, 0.001].

The architecture of the neural networks comprises two layers with 126 neurons each, followed by three layers with 256 neurons each, and two additional layers with 126 neurons each. Finally, there is a dense layer with 7 neurons. The activation function for the hidden layers is the ReLU function, and we apply a dropout rate of 0.2 between layers. The training was conducted in the TensorFlow environment using the Adam optimizer with a learning rate of 10^{-4} for 2000 epochs [14]. Again the hyperparameters have been selected during the data collection phase. We tested different architectures: we tried architectures with between 3 and 10 layers and 32 and 512 neurons; ReLU and tanh activation functions, learning rate between 10^{-2} and 10^{-6}, and epochs up to 3000.

3. Results and Discussion

In this section, we present the results related to the approximation model.

We used a dataset of 14000 samples to train our XGboost and neural network models. We randomly split this dataset into two parts: 13200 samples for training and 800 samples for independent evaluation. The results are shown in Table 2.

Table 2 Comparison of the XGboost and neural network models performance

Mean absolute error	XGboost	Neural network
Depth (µm)	1.6	3.2
Width (µm)	52	362
Burr1 (µm)	0.20	0.22
Burr2 (µm)	0.23	0.25
Angle1 (°)	4.9	22.1
Angle2 (°)	5.0	22.0
Sa(µm)	0.23	0.33

As indicated in Table 2, the XGboost outperforms the neural network model. This result is not surprising given that the XGboost model is known to provide better performance for tabular data, as we have, than the neural network. Therefore, the next part of this section will focus on the results obtained by the most efficient AI system.

Error analysis revealed that a significant portion of the error stemmed from the data collection process. Indeed, given that the sets of engraving parameters are generated randomly, some input parameters correspond to poor machining quality and/or measurement issues. In these cases, the data points were labeled as warnings in our dataset, and the output values for depth, width, burrs, and angles were reset to a default value of 0. It is important to note that for

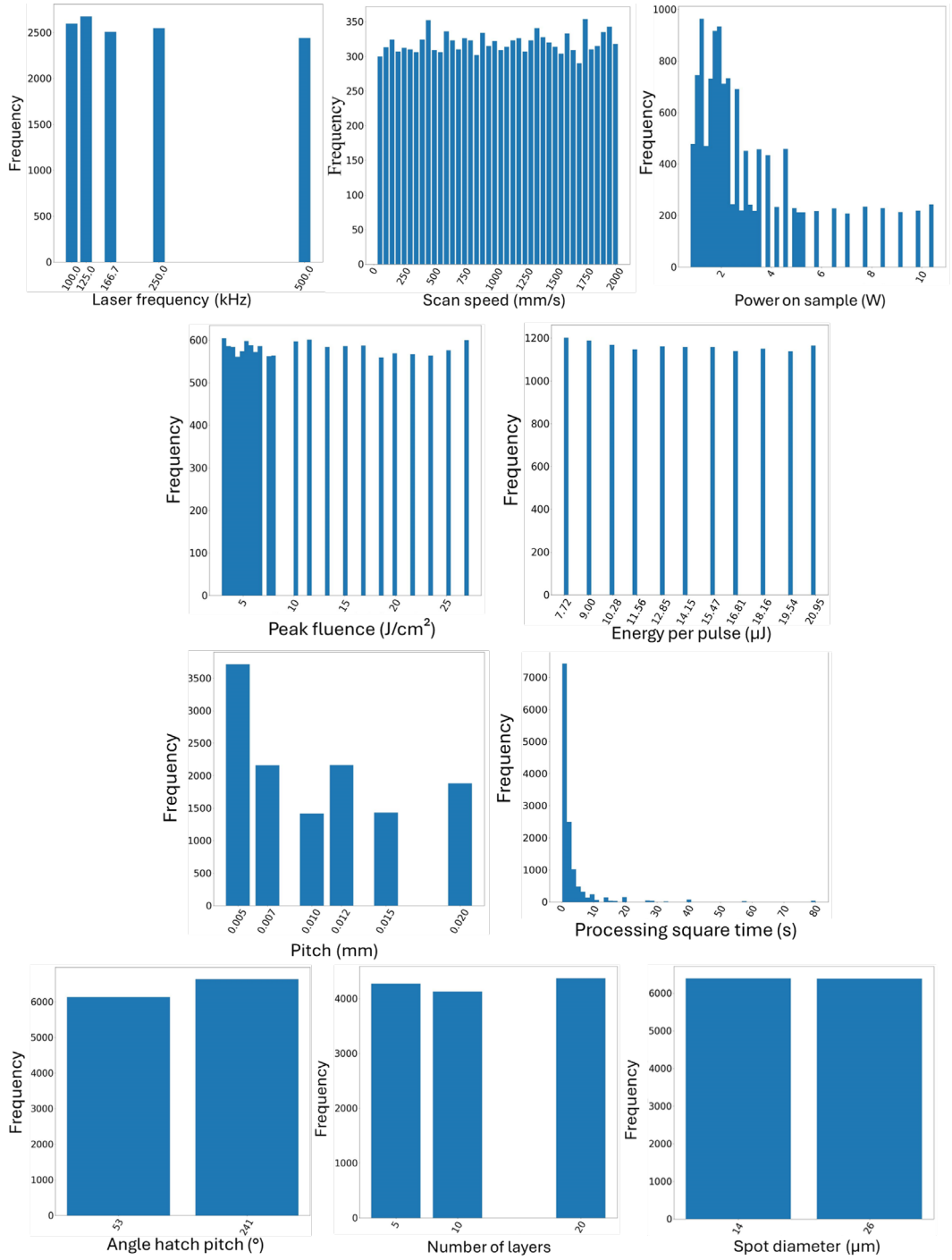

Fig. 3 Histogram plots showing the frequency distribution of the input parameters of the AI algorithm (XGboost or neural networks).

these points, the actual depth and other output parameters might be nonzero. Consequently, the metrics are penalized when the model correctly predicts the real engraving properties. Additionally, it is desirable to make the distinction between warning and safe parameters. To address this, we built a classifier based on our model. The width prediction is used to classify our data points into two categories: warning and safe. All inputs whose width prediction is less than 500 μm is classified as a warning. This classification method achieves an accuracy of 97% as presented in Table 3. We recall that accuracy measures how often the classifier is correct overall. In addition, we report recall and precision: recall is the percentage of actual warning/safe points correctly identified, and precision is the percentage of predicted warnings that are actual warning/safe points. These metrics are given in Table 3.

Table 3 Performance report of the classifier

	Precision	Recall	Number of tested sample
Warning	0.8	0.33	36
Safe	0.97	0.99	764
Accuracy			0.97

For the predicted warnings, we then set the predicted values for depth, width, burrs, angles, and surface roughness to zero. This improves the overall performance of the model as shown in Table 4. This approach yielded our best performance and the Fig. 5 illustrates a comparison between the measured and predicted depth and surface roughness. The plots for the other output parameters are available in Appendix A.

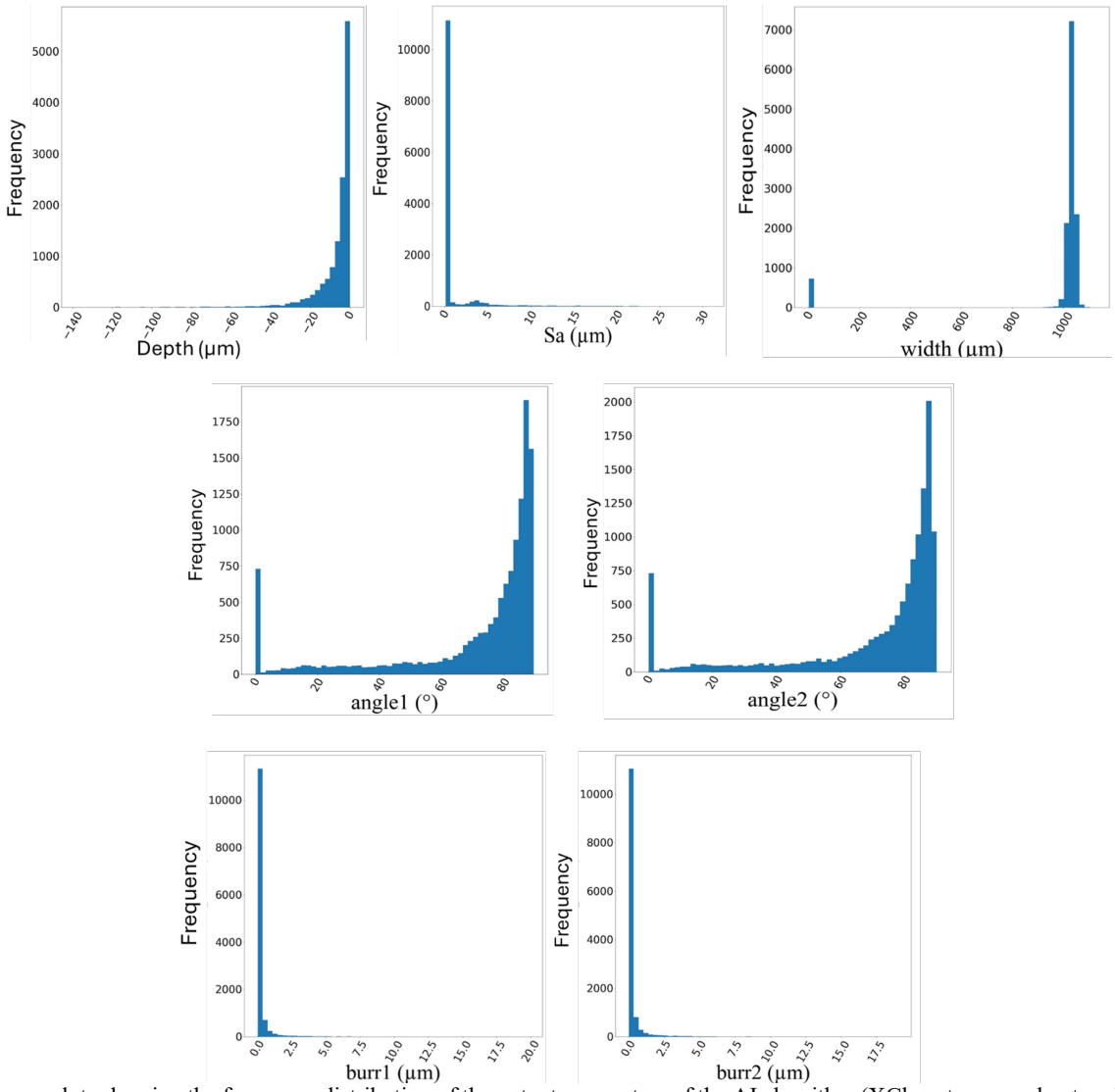

Fig. 4 Histogram plots showing the frequency distribution of the output parameters of the AI algorithm (XGboost or neural networks).

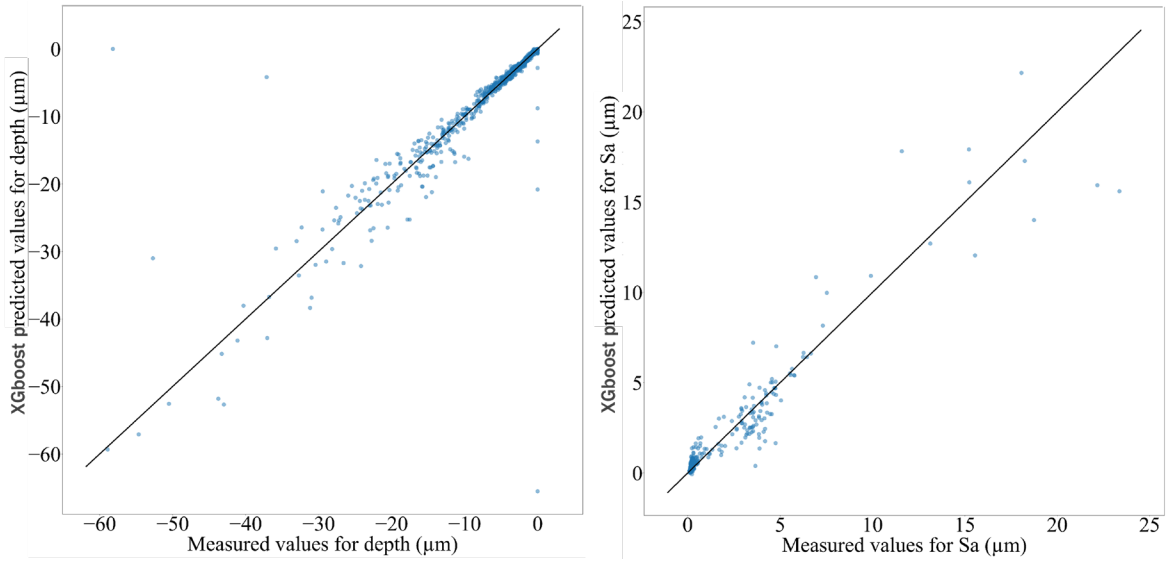

Fig. 5 Measured and XGboost predicted depth and surface roughness on the test set.

Table 4 Comparison of the model performance with and without classifier

Mean absolute error	Without	With
Depth (µm)	1.6	1.4
Width (µm)	52	51
Burr1 (µm)	0.20	0.19
Burr2 (µm)	0.23	0.22
Angle1 (°)	4.9	4.7
Angle2 (°)	5.0	4.9
Sa(µm)	0.23	0.23

The current performances of the AI model are presented in the form of error bars plots in Fig. 6. The plots for the other output parameters are available in Appendix B.

In terms of mean percentage error, the performances of the XGboost are 12%, 3%, 7%, 6%, 33%, 345 %, and 276% for the depth, width, angle 1, angle 2, surface roughness, burr 1, and burr 2, respectively. It should be noted that the error is not uniformly distributed across samples of different sizes. Indeed, samples with large depths and uncertain measurements (warnings) exhibit a much larger error. For large depths, the error can be explained by the rarity of these configurations in usable measured data, which occur in only about 5% of cases. The zero-depth error corresponds to warnings. Additionally, we observed that the performance of the model for burrs predictions is much lower than for the other engraving properties. This observation is not surprising given that the burrs are partly linked to thermal effects which have a stochastic nature. In addition, in terms of absolute value, the high mean percentage for the burrs corresponds to 0.19 µm and 0.22 µm for burr 1 and burr 2, respectively. These values are acceptable given that these are closed to the initial surface roughness and to the minimum measurable surface roughness (0.10 µm).

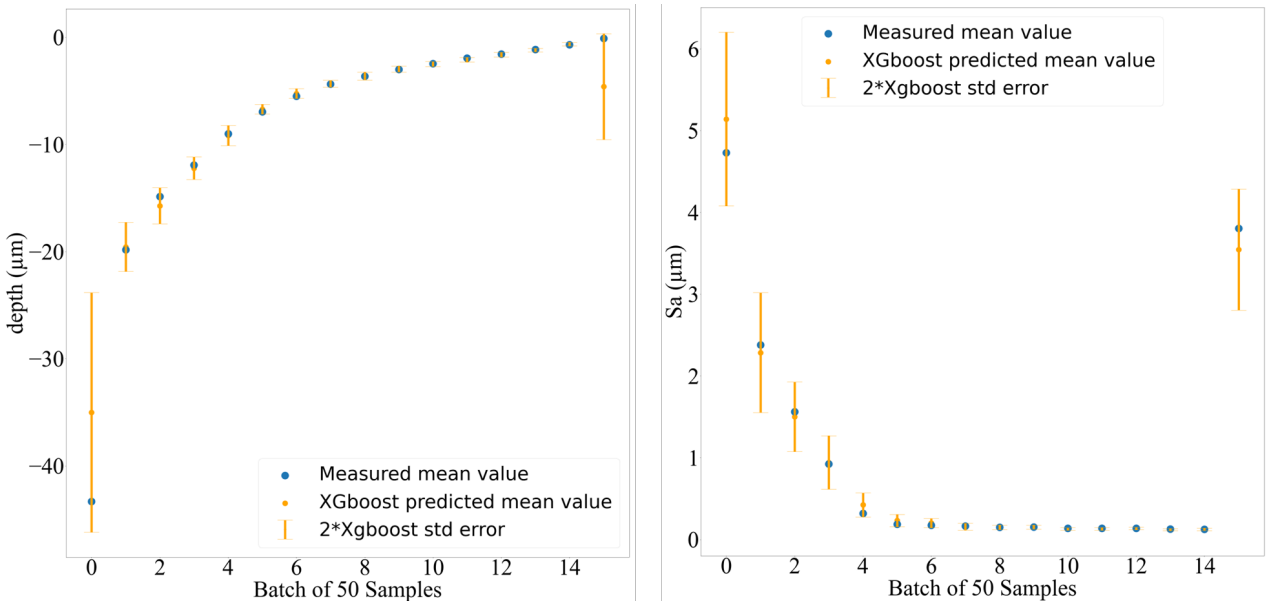

Fig. 6 Measured mean values for depth and surface roughness on batch of 50 samples as well as the associated XGboost predicted mean values and the XGboost standard deviations (XGboost std error). Samples are ordered from greatest to least depth.

To evaluate the performance of the AI model to the predictions that can be made by a simulator based on theoretical physical models, a comparison is made between the AI system and our LS-Plume® simulator [18]. The Table 5 presents the comparison of both models' performances evaluated on the same set of samples. The simulator does not predict thermal effects. Consequently, the performance for the burrs and the surface roughness estimations are not presented.

The Fig. 7 shows a comparison of the predicted depth with the XGboost model and the LS-Plume®. The plots for the other output parameters are available in Appendix C. The simulator performances are already quite good but the XGboost model allowed an improvement in prediction performances. Indeed, from the information provided in Table 5, it can be seen that the simulator has a mean percentage error of 36%, 2%, 13%, and 12 % for the depth, width, angle 1, and angle 2, respectively. As mentioned before, the mean percentage errors for the XGboost predictions are 12%, 3%, 7%, and 6%, for the depth, width, angle 1, and angle 2, respectively. Consequently, the AI model increases the accuracy of predictions for depth and angles.

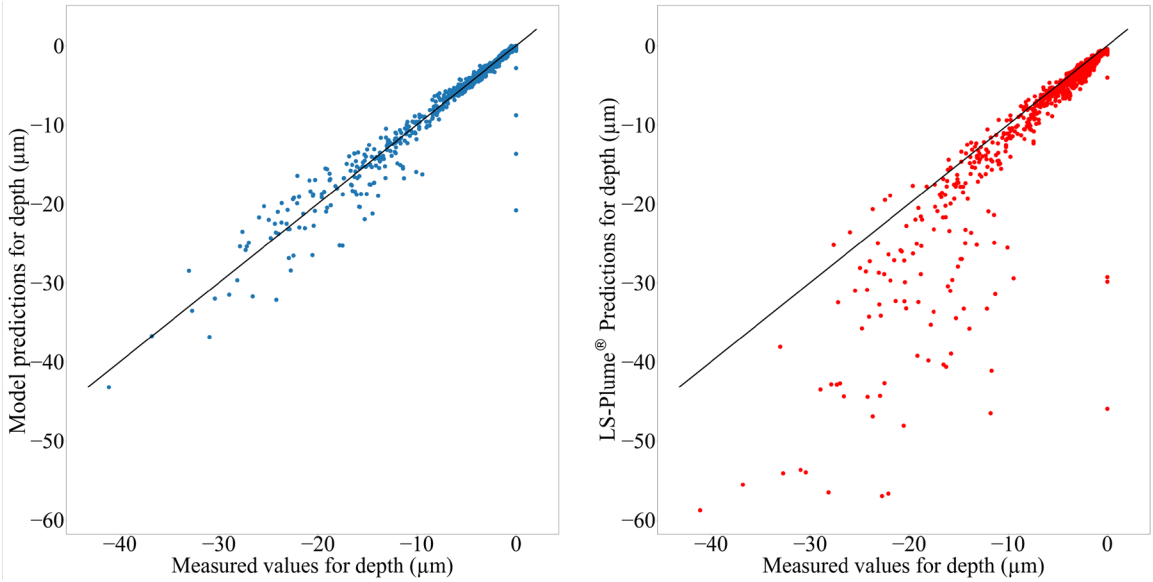

Fig. 7 Comparison between the prediction of the XGboost (left graph) and the profile simulator LS-Plume® (right graph) for the depth.

Table 5 Comparison of the performance of the XGboost model and the LS-Plume® simulator

Metrics	Mean	Mean absolute error XGboost	Mean absolute error LS-Plume®
Depth (µm)	8.2	1.4	5.6
Width (µm)	1000	51	67
Angle1 (°)	70.0	6.6	9.6
Angle2 (°)	70.3	5.7	9.6

4. Conclusion and outlooks

In recent years, the use of artificial intelligence has become more and more important in many areas, including in the world of laser micromachining. Our work is part of this evolution of new generations of tools by proposing to combine the know-how of experts in laser micromachining and the predictions of an artificial intelligence model trained with real data for engraving processes. The parameter space explored by the real data is made up of ten engraving parameters: laser frequency, laser power, energy per pulse, spot diameter, peak fluence, scanning speed, spacing between machining lines, number of machining layers, angle between each layer, and physical machining time of a square. For each of them, several discrete values are available and chosen based on common values found in industrial applications. The large amount of input parameters of the AI model requires a large amount of real data for the AI training phase. To meet this requirement, we developed an automated square machining procedure with a random combination of these input parameters and an automated measurement phase using an Alicona microscope to obtain the engraving properties: depth, width, surface roughness, angles, and burrs. All of these parameters for 13200 machined squares of 1x1 mm² allow to train two types of AI models: the XGboost and the neural network to obtain an approximation function of the physical system to predict the machining characteristics from the engraving parameters. The XGboost algorithm outperforms the neural network model as expected for tabular data. Our AI model achieves an average precision of 12%, 3%, 33%, 7%, 6%, 345%, and 276% for depth, width, surface roughness, angle 1, angle 2, burr 1, and burr 2, respectively. The approximation function is then used by a genetic algorithm to make the inversion, work included in the EP 3 743 236 B1 patent [19], and obtain good candidates of optimal laser parameters distributed in the parameter space to meet quality criteria for any application. An operator will be able to eliminate some of them based on his experience and select the best one amongst others for the intended application. This new tool saves significant time and samples since it eliminates the entire parameter research phase usually carried out for each new process to be developed. This AI system, apart from avoiding a test-error phase until the desired simulated profile is obtained, also presents increased performance compared to our LS-Plume® simulator with an improvement in average precision of 24%, 3%, 2% for depth, angle 1, and angle 2, respectively. In addition, the AI model offers predictions of surface roughness and burrs.

This proof of concept was carried out for 316L stainless steel. Before carrying out machine learning of other materials, the performance of the current model will be improved by generating data for extremes cases such as significant engraving depths to improve the knowledge of the AI model in these regions. It is also planned to expand the explored engraving parameter space.

This innovative tool opens the door to on one hand improving laser micromachining both in terms of quality and cycle time, and on the other hand to democratize highly complex phenomena (including stochastic) to easy to use and first time right processes and results.

Acknowledgments

The authors would like to acknowledge the financial support of the Wallonia Region, Belgium, in the frame of the NAVIC project, with convention number 8660.

Appendix A

The Fig. 8 presents the measured and predicted width, angle 1, and angle 2.

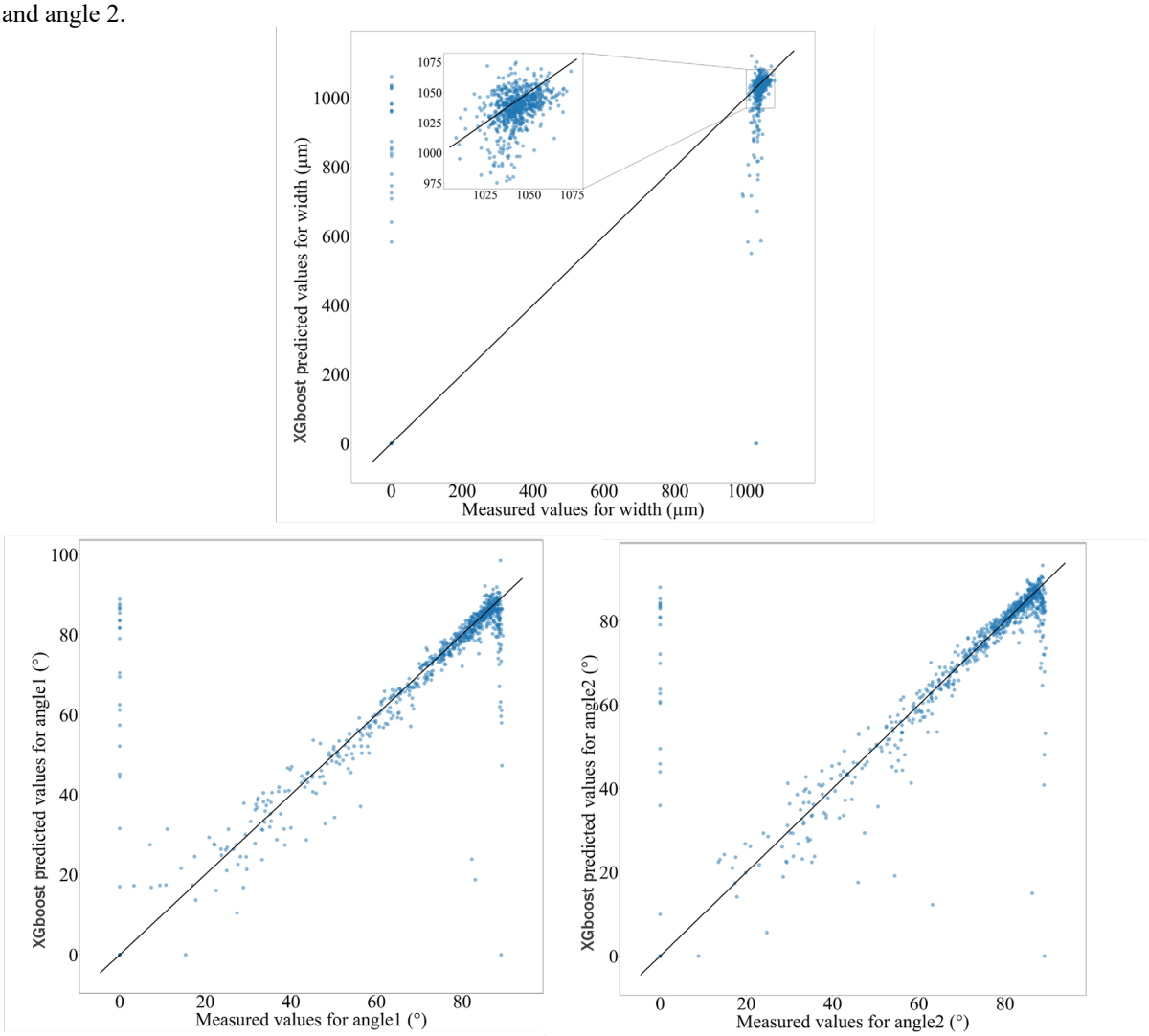

Fig. 8 Measured and XGboost predicted width, angle 1, and angle 2 on the test set.

The Fig. 9 depicts the measured and predicted burrs 1 and 2.

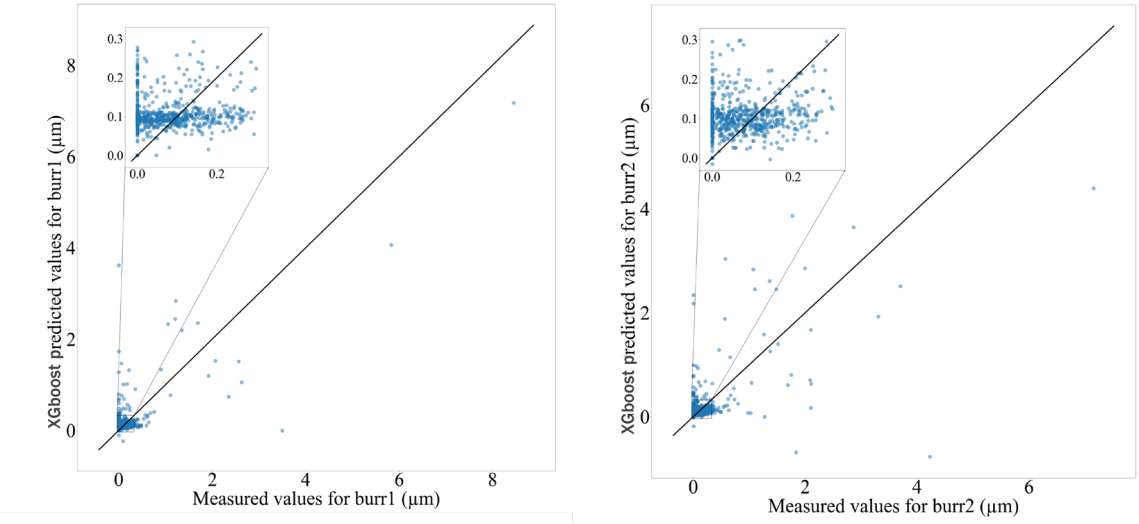

Fig. 9 Measured and XGboost predicted burrs 1 and burrs 2 on the test set. Samples are ordered from greatest to least depth.

Appendix B

The Fig. 10 shows the error bars plots for the width, angle 1, and angle 2.

The Fig. 11 depicts the error bars plots for burrs 1 and 2.

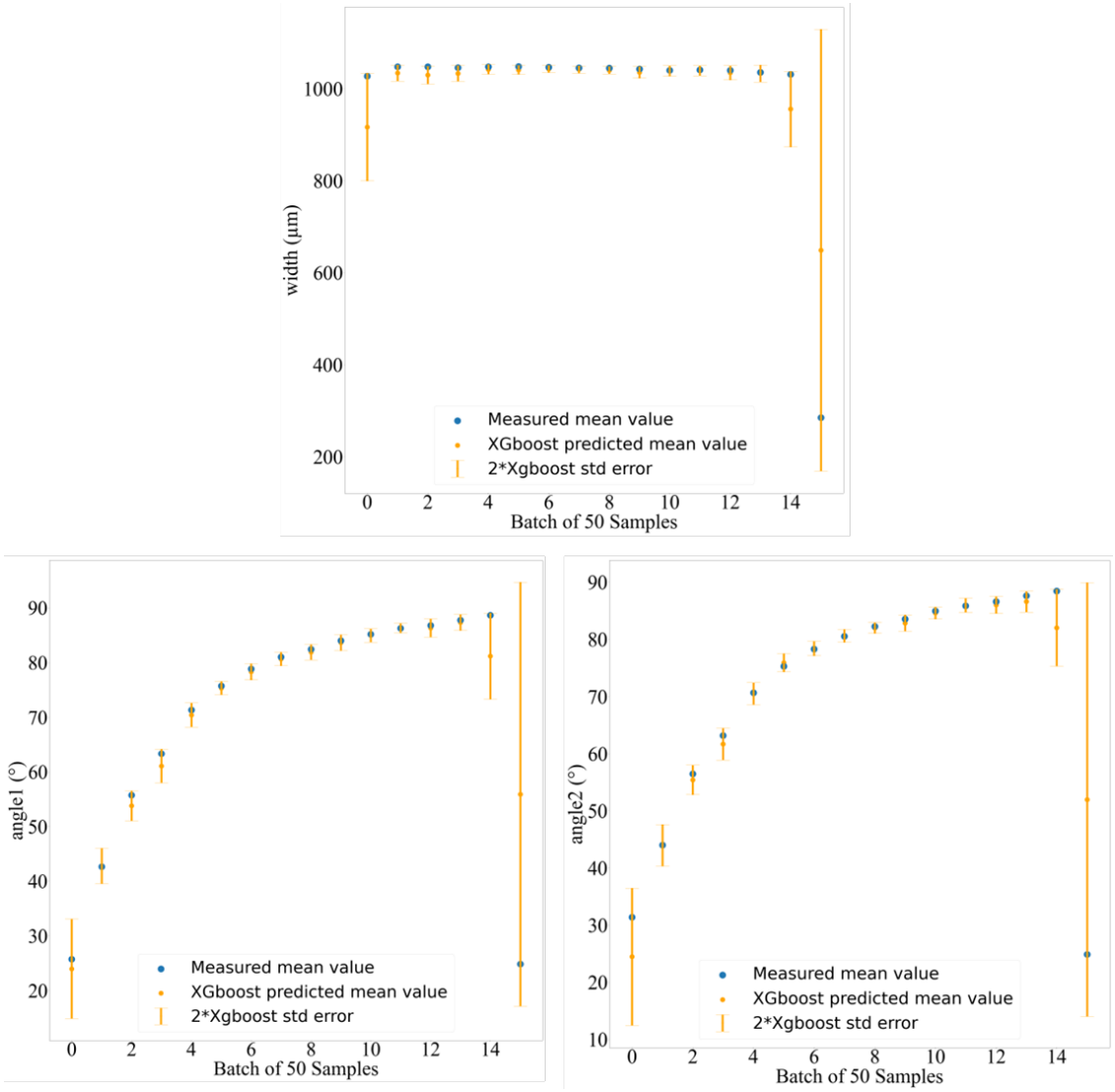

Fig. 10 Measured mean values for width, angle 1, and angle 2 on batch of 50 samples as well as the associated XGboost predicted mean values and the XGboost standard deviations (XGboost std error). Samples are ordered from greatest to least depth.

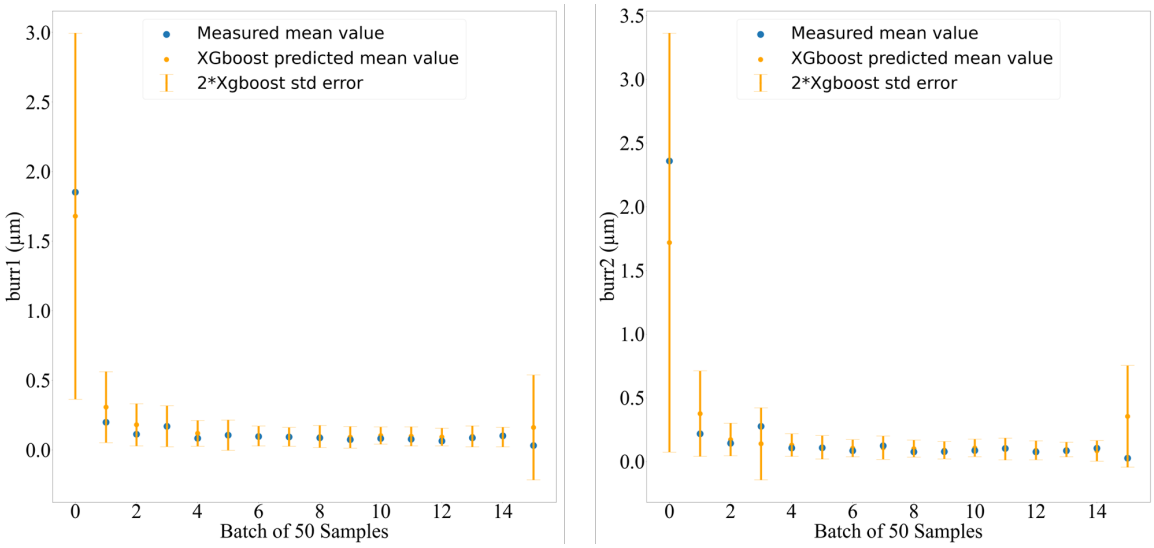

Fig. 11 Measured mean values for burr 1 and burr 2 on batch of 50 samples as well as the associated XGboost predicted mean values and the XGboost standard deviations (XGboost std error). Samples are ordered from greatest to least depth.

Appendix C

The Fig. 12 shows a comparison of the predicted width with the XGboost model and the LS-Plume®. The Fig. 13 and Fig. 14 present this comparison for angle 1 and angle 2, respectively.

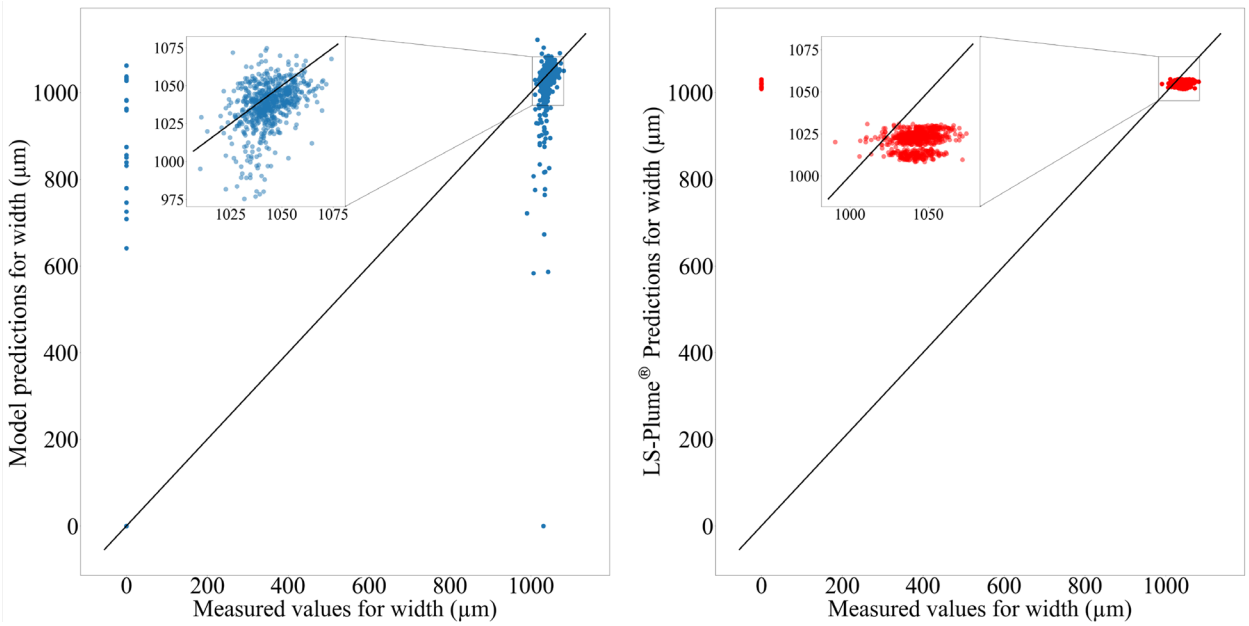

Fig. 12 Comparison between the prediction of the XGboost model (left graph) and the profile simulator LS-Plume® (right graph) for the width.

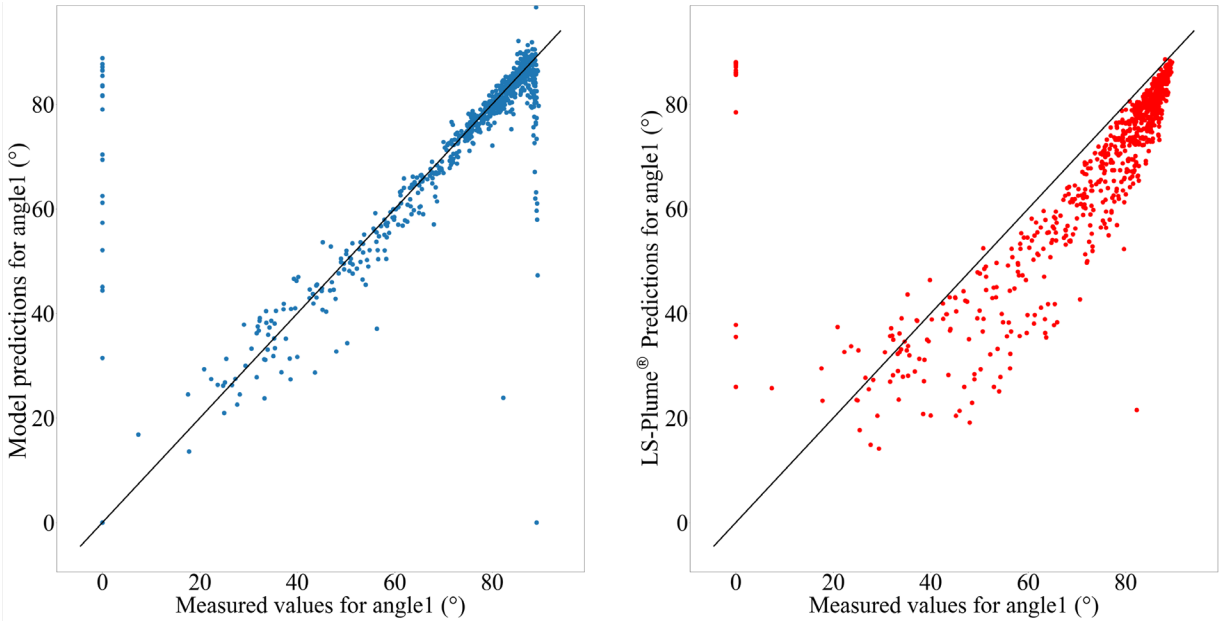

Fig. 13 Comparison between the prediction of the XGboost model (left graph) and the profile simulator LS-Plume® (right graph) for the angle 1.

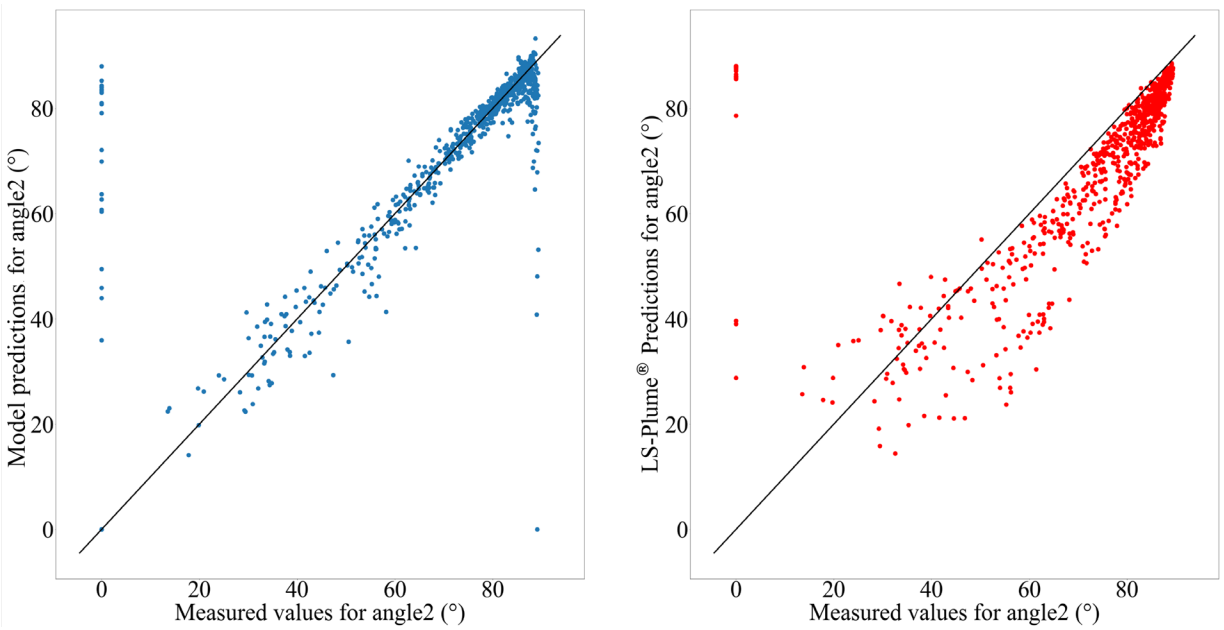

Fig. 14 Comparison between the prediction of the XGboost model (left graph) and the profile simulator LS-Plume® (right graph) for the angle 2.

References

[1] R. Le Harzic, N. Huot, E. Audouard, C. Jonin, P. Laporte, S. Valette, A. Fraczkievic, and R. Fortunier: Appl. Phys. Lett., 80, (2002) 3887.

[2] B.N. Chichkov, C. Momma, S. Nolte, F. von Alvensleben, and A. Tünnerman: Appl. Phys. A, 63, (1996) 109.

[3] W. Kautek and J. Krueger: Proc. SPIE, Vol. 2207, (1994) 600.

[4] B. Neuenschwander, B. Jaeggi, and M. Schmid: Proc. ICALEO 2012, (2012) 1004.

[5] K.M Davis, K. Miura, N. Sugimoto, and K. Hirao: Optics Letters, 21, (1996) 1729.

[6] D.S. Correa, M. R. Cordoso, V. Tribuzi, L. Misoguti, and C.R. Mendonca: IEEE Journal of Selected Topics in Quantum Electronics, 18, (2012) 176.

[7] J. Heitz, C. Plamadeala, M. Muck, O. Armbruster, W. Baumgartner, A. Weth, C. Steinwender, H. Blessberger, J. Kellermair, S.V. Kirner, J. Krüger, J. Bonse, A.S Guntner, and A.W. Hassel: Appl. Phys. A, 123, (2017) 734.

[8] P.E. Martin, S. Estival, M. Dijoux, A. Kupisiewicz, and R. Braunschweig : J. Laser Appl., 29, (2017) 022211.

[9] S. Singh and G.L Samuel: Proc. Materials Today, (2023) S22147853230291.

[10] K. Sugioka and Y. Cheng: Light Sci. Appl., 3, (2014) e149.

[11] L. Cangueiro, J.A. Ramos-de-Campos, and D. Bruneel : Molecules, 26, (2021) 6327.

[12] P. Vanwersch, B. Nagarajan, A. Van Bael, and S. Castagne: Micromachines, 14, (2023) 593.

[13] T. Chen and C. Guestrin: Proc. The 22nd ACM SIGKDD International conference on Knowledge Discovery and Data Mining (2016) 785.

[14] T. Hastie, R. Tibshirani, and J. Friedman: "The element of Statistical Learning", (Springer, New York, 2009) p. 337.

[15] B. Mills and J.A. Grant-Jacob: IET Optoelectron., 15, (2021) 207.

[16] X. Ren, J. Fan, R. Pan, and K. Sun: The international Journal of Advanced Manufacturing Technology, 127, (2023) 1177.

[17] M.D.T McDonnell, D. Arnaldo, E. Pelletier, J.A. Grant-Jacob, M. Praeger, D. Karnakis, R.W. Eason, B. Mills: Journal of Intelligent Manufacturing, 32, (2021) 1471.

[18] S.A. Lasea: "LS-Plume", (2020). Available online: https://www.ls-plume.com/ (accessed on 6 June 2024).

[19] D. Bruneel, L. Cangueiro, P.E. Martin, J.A. Ramos De Campos, and A. Kupisiewicz: European Patent Office EP3743236B1 (2019).

(Received: June 29, 2024, Accepted: May 17, 2025)